Ashkin-Teller model and diverse opinion phase transitions on multiplex networks

S. Jang,[1] J. S. Lee,[2] S. Hwang,[3,4] and B. Kahng[3]
[1]*Department of Physics and Chemistry, Korea Military Academy, Seoul 139-804, Korea*
[2]*School of Physics, Korea Institute for Advanced Study, Seoul 130-722, Korea*
[3]*CCSS, CTP, Department of Physics and Astronomy, Seoul National University, Seoul 151-747, Korea*
[4]*Institute for Theoretical Physics, University of Cologne, 50937 Köln, Germany*
(Received 3 October 2014; revised manuscript received 16 June 2015; published 7 August 2015)

Multiplex networks (MNs) have become a platform of recent research in network sciences because networks in many real-world systems interact and function together. One of the main scientific issues in MNs is how the interdependence changes the emerging patterns or phase transitions. Until now, studies of such an issue have concentrated on cluster-breakdown phenomena, aiming to understand the resilience of the system under random failures of edges. These studies have revealed that various phase transition (PT) types emerge in MNs. However, such studies are rather limited to percolation-related problems, i.e., the limit $q \to 1$ of the q-state Potts model. Thus, a systematic study of opinion formation in social networks with the effect of interdependence between different social communities, which may be seen as the study of the emerging pattern of the Ising model on MNs, is needed. Here we study a well-known spin model called the Ashkin-Teller (AT) model in scale-free networks. The AT model can be regarded as a model for interacting systems between two species of Ising spins placed on respective layers in double-layer networks. Our study shows that, depending on the interlayer coupling strength and a network topology, unconventional PT patterns can also emerge in interaction-based phenomena: continuous, discontinuous, successive, and mixed-order PTs and a continuous PT not satisfying the scaling relation. The origins of such rich PT patterns are elucidated in the framework of Landau-Ginzburg theory.

DOI: 10.1103/PhysRevE.92.022110 PACS number(s): 05.70.Fh, 05.90.+m, 89.75.Da

I. INTRODUCTION

In the past decade a surge of scientific interest has been directed at studying emerging phenomena in complex systems. These include various cooperative phenomena such as blackouts of power systems [1], spreading of disease [2,3], and formation of opinion [4,5]. In these phenomena, macroscopic patterns or phases emerge via the interactions between individual components. Therefore, the fundamental question about these phenomena is how to understand the origin of various emerging phases and the transition nature between the phases. In the early stage of these studies, this question was mainly investigated in terms of a single complex system and its topological effects was a central issue. However, many complex networks in real-world systems are in fact interdependent and it was found that such interdependence can also affect the emerging patterns significantly [1,6]. This finding triggered extensive studies on emerging phenomena on multiplex (or interdependent) networks (MNs) [7–9]. Here the MN is a network of networks in which nodes on one network are identical to those on another network.

Such effect of MNs were first investigated for the cluster-breakdown phenomena in the framework of percolation theory [1,6]. In these studies, the robustness of a complex network system is investigated by removing edges or nodes in a complex network system. Here the fraction of nodes in a remaining giant component is the order parameter for percolation transition. This order parameter is reduced to zero as the number of removed edges or nodes is increased beyond a certain percolation threshold. Then a percolation transition takes place, which is conventionally continuous in a monolayer network [9]. However, it was found that the abrupt transition can occur in MNs. For example, failure of a node in one network can cause failure of nodes in the other networks, leading to cascading back-and-forth failures [1]. Then a discontinuous phase transition (PT) occurs. Thereafter, variations of the percolation model to study the resilience of MNs were proposed and richer PT patterns emerged; an even mixed-order (or hybrid) PT [6,10,11] was reported. Here the mixed-order PT is the transition where features of both continuous and discontinuous PTs appear at the same transition point. Note that the mixed-order PT has been found in several physical models, such as the bootstrap model [12], jamming percolation [13,14], the Ising model with long-range interactions [10], the synchronization model [15], and the percolation transition on multiplex networks [6].

Besides percolation phenomena, one can also expect that interdependence of social networks diversifies the emerging PT patterns and sometimes induces an unexpected PT in general interaction-based phenomena [16]. This expectation can be supported by the recent revolutionary wave that occurred in the Middle East and North Africa, called Arab Spring. In this movement, strengthened interactions between civil societies in different nations via social media have an important role causing avalanching revolutions, which is unprecedented. This example clearly shows that PT patterns of social phases could be significantly affected by the interdependence of networks.

Since such interdependence is expected to be stronger in the future, it is of crucial importance to systematically investigate the effect of interdependence as well as the topology of the network on PT patterns for opinion-formation phenomena in MNs. For this investigation, the Ising model is a proper one, which has been used to study the problems of opinion formation in social networks and is often analytically solvable. Each spin direction of the Ising model represents one of two opposite opinions in social issues. Examples include the Sznajd model [4] and the voter model [5]. We remark that most studies focus on the dynamics of opinion formation. However, here we are interested in a phase diagram created by the Ising

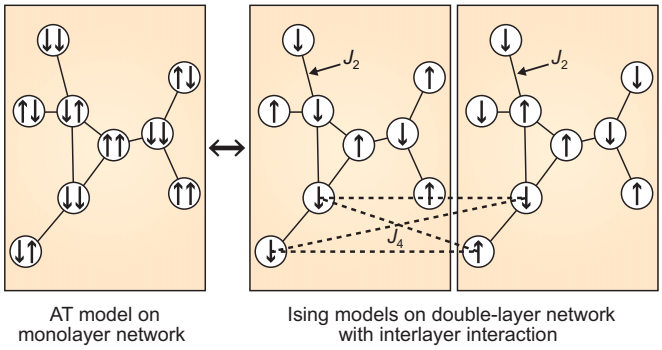

FIG. 1. (Color online) The AT model on a monolayer network can be regarded as a two-species-of-Ising-spin model with an interlayer interaction (dashed lines) on a double-layer network. Here two identical layers form this multiplex networks and the coupling between these layers are realized by the four-spin coupling attached to each link.

model on MNs, which is helpful in understanding diverse patterns created through the dynamics of opinion formation in a single framework. Those studies were carried out mostly on monolayer networks; however, a few of them have been extended to the case on multilayer networks [17,18]. Suchecki and Hołyst [19] also studied the Ising model on a double-layer MN. Interestingly, it exhibited a discontinuous PT, whereas it shows a continuous PT in a monolayer network. These results led us to speculate that the pattern of the PT can be changed systematically by controlling the interlayer coupling strength; in the above examples, zero coupling strength (no connection) results in a continuous PT, whereas finite coupling strength leads to a change in PT type to a discontinuous PT. However, a systematic understanding of it has been absent thus far.

To systematically understand the role of interdependence as well as the topology of a network in a single framework, here we study an Ising spin model called the Ashkin-Teller (AT) model [20] on monolayer scale-free (SF) networks. The AT model contains two species of Ising spins: the s spin and the σ spin. We want to regard these as a single species of Ising spin placed on the respective layers of a double-layer MN with interlayer interaction, as shown in Fig. 1. By controlling the strength of the interlayer interaction and the topology of a network, the change in PT type is investigated systematically. By applying Landau-Ginzburg theory to the AT model on SF networks, we obtain a rich phase diagram containing the paramagnetic, Baxter (ferromagnetic), and so-called $\langle \sigma s \rangle$ phases (in which the product of the σ and s spins is ordered, but $\langle s \rangle = \langle \sigma \rangle = 0$). The PTs between those phases also include diverse types: continuous, discontinuous, successive (a discontinuous jump in the order parameter after continuous PT), and mixed-order PTs. These intriguing diverse patterns of PTs originate from the unconventional extension of the first-order PT lines in the phase diagram. In particular, such an extension creates the critical end (CE) points, where the mixed-order PT occurs. Finally, by calculating the critical exponents explicitly, we find that the PT of the product of the σ and s spins does not satisfy the scaling relations even at the continuous PT point.

II. MODEL AND FORMALISM

Let us start by introducing the AT model specifically. Two species of Ising spins, s_i and σ_i with states $s_i = \pm 1$ and $\sigma_i = \pm 1$, respectively, are placed at each node i, as shown in Fig. 1. The Hamiltonian of the AT model without an external field, denoted by $\mathcal{H}_o$, is represented as

$$-\beta \mathcal{H}_o = K_2 \sum_{\langle i,j \rangle} s_i s_j + K_2 \sum_{\langle i,j \rangle} \sigma_i \sigma_j + K_4 \sum_{\langle i,j \rangle} s_i \sigma_i s_j \sigma_j, \quad (1)$$

where $\beta = 1/k_B T$ with the Boltzmann constant k_B and temperature T, $K_2 = \beta J_2$ and $K_4 = \beta J_4$ with coupling constants J_2 and J_4, and $\langle i,j \rangle$ runs over all pairs of nodes connected by links. We study the AT model on the SF network, which is a random graph where each node has a heterogeneous number of connections, referred to as degree k, following the power law $P_d(k) = N_\lambda k^{-\lambda}$. The coupling between the two layers is shaped in the form of the four-spin interaction with the coupling constant J_4. Thus, the topology and the interdependence of a network can be controlled by two parameters, λ and $x \equiv J_4/J_2$, respectively.

We now calculate the mean-field free energy for the Hamiltonian (1). The local order parameter acting on the spins s, σ, and $s\sigma$ at node i are, respectively, referred to as m_s^i, m_σ^i, and $m_{s\sigma}^i$, where $m_s^i = \langle s_i \rangle$, $m_\sigma^i = \langle \sigma_i \rangle$, and $m_{s\sigma}^i = \langle s\sigma_i \rangle$. Here $\langle \cdots \rangle$ is the ensemble average of a given quantity. Next we expand each spin about the local order parameter as $s_i = m_s^i + \delta m_s^i$, $\sigma_i = m_\sigma^i + \delta m_\sigma^i$, and $s\sigma_i = m_{s\sigma}^i + \delta m_{s\sigma}^i$. By neglecting the higher-order terms in δm_s^i, δm_σ^i, and $\delta m_{s\sigma}^i$, the mean-field Hamiltonian $\mathcal{H}_{\rm MF}$ is rewritten as

$$-\beta \mathcal{H}_{\rm MF} \simeq -K_2 \sum_{\langle i,j \rangle} \left(m_s^i m_s^j + m_\sigma^i m_\sigma^j \right) - K_4 \sum_{\langle i,j \rangle} m_{s\sigma}^i m_{s\sigma}^j + K_2 \sum_{\langle i,j \rangle} 2 m_\sigma^j (s_i + \sigma_i) + K_4 \sum_{\langle i,j \rangle} 2 m_{s\sigma}^j s_i \sigma_i. \quad (2)$$

Then the mean-field free energy $\mathcal{F}$ is obtained as

$$\beta \mathcal{F} = -\ln Z \simeq -\ln \sum_{\{s_i, \sigma_i\}} e^{-\beta \mathcal{H}_{\rm MF}} = -\sum_i \ln Z_i + K_2 \sum_{\langle i,j \rangle} \left(m_s^i m_s^j + m_\sigma^i m_\sigma^j \right) + K_4 \sum_{\langle i,j \rangle} m_{s\sigma}^i m_{s\sigma}^j, \quad (3)$$

where

$$Z_i = 4[c^i(s) c^i(\sigma) c^i(s\sigma) + s^i(s) s^i(\sigma) s^i(s\sigma)], \quad (4)$$

with $c^i(\alpha) \equiv \cosh(\sum_{j(i)} K_2 m_\alpha^j)$ and $s^i(\alpha) \equiv \sinh(\sum_{j(i)} K_2 m_\alpha^j)$ for $\alpha = s$ and σ. $c^i(s\sigma) \equiv \cosh(\sum_{j(i)} K_4 m_{s\sigma}^j)$ and $s^i(s\sigma) \equiv \sinh(\sum_{j(i)} K_4 m_{s\sigma}^j)$. Here $\sum_{j(i)}$ denotes that the summation runs over all nearest neighbors j of node i.

In order to make the summation tractable, we used the annealed network approximation $\sum_{\langle i,j \rangle} \mathcal{A}_{ij} \to \sum_{i \neq j} \frac{k_i k_j}{2N\langle k \rangle} \mathcal{A}_{ij}$, where N is the total number of nodes, $\langle k \rangle$ is the mean degree of a network, and $\mathcal{A}_{ij}$ is a given function of i and j. Such an annealed approximation has proven to yield reasonable results of various critical phenomena in complex networks [21,22].

We also used the global magnetization m_α as $m_\alpha = \sum_i k_i m_\alpha^i / N\langle k \rangle$, where α represents either s, σ, or $s\sigma$. Then we set $m_s = m_\sigma \equiv m$ and $m_{s\sigma} \equiv M$, taking advantage of the

symmetry $\sigma \leftrightarrow s$. The two order parameters m and M, in the AT model, will be referred to as m magnetization and M magnetization, respectively.

By rewriting the free energy in terms of m and M after the annealed approximation, $f \equiv \beta\mathcal{F}/N$ is given by

$$f \simeq -2\int_{k_{\min}}^{\infty} \ln[\cosh(K_2 mk)]P_d(k)dk - \int_{k_{\min}}^{\infty} \ln[\cosh(K_4 Mk)]P_d(k)dk - \mathcal{B}_1 + K_2 m^2\langle k\rangle + \frac{1}{2}K_4 M^2\langle k\rangle, \quad (5)$$

where

$$\mathcal{B}_1 = \int_{k_{\min}}^{\infty} \ln[1+\tanh^2(K_2 mk)\tanh(K_4 Mk)]P_d(k)dk. \quad (6)$$

The minimization conditions $\frac{\partial f}{\partial m} = 0$ and $\frac{\partial f}{\partial M} = 0$ lead to the following self-consistent relations:

$$m\langle k\rangle = \int_{k_{\min}}^{\infty} \frac{\tanh(K_2 mk)[1+\tanh(K_4 mk)]}{1+\tanh^2(K_2 mk)\tanh(K_4 Mk)} k P_d(k)dk \quad (7)$$

and

$$M\langle k\rangle = \int_{k_{\min}}^{\infty} \frac{\tanh(K_4 Mk)+\tanh^2(K_2 mk)}{1+\tanh^2(K_2 mk)\tanh(K_4 Mk)} k P_d(k)dk. \quad (8)$$

There exist three possible solutions for Eqs. (7) and (8): the paraphase ($m = M = 0$), the Baxter phase ($m, M > 0$), and the $\langle\sigma s\rangle$ ($m = 0$ and $M > 0$) phase. However, the condition $m > 0, M = 0$ cannot satisfy the above relations.

To obtain the susceptibility, we also consider an AT Hamiltonian with an external field, which is written as

$$-\beta\mathcal{H} = -\beta\mathcal{H}_o + \sum_i k_i H_2(s_i+\sigma_i) + \sum_i k_i H_4 s_i\sigma_i, \quad (9)$$

where the external fields H_2 and H_4 are weighted by the degree of each node. Then the relations between the free energy and magnetization hold $-\partial f/\partial H_2 = 2m\langle k\rangle$ and $-\partial f/\partial H_4 = M\langle k\rangle$. The corresponding free energy and self-consistent relations are simply given by the substitution of $K_2 mk$ and $K_4 Mk$ in the integrations of Eqs. (5)–(8) to $(K_2 m + H_2)k$ and $(K_4 M + H_4)k$, respectively [see Eqs. (B1) and (B2)]. Next, by taking the partial derivative of m (M) with respect to H_2 (H_4) and then taking the limit $H_2, H_4 \to 0$, we obtain the susceptibilities $\chi_m \equiv \partial m/\partial H_2|_{H_2,H_4\to 0}$ ($\chi_M \equiv \partial M/\partial H_4|_{H_2,H_4\to 0}$).

III. RESULTS

In this section we begin by describing the schematic phase diagrams obtained for the AT model to provide an overview to the reader. Figures 2(a) and 2(b) show schematic phase diagrams in the parameter space $(x \equiv J_4/J_2, T^{-1})$ for $\lambda_c < \lambda < 4$ ($\lambda_c \approx 3.503$) and (x,λ) for $3 < \lambda < 4$, respectively, obtained based on the criteria discussed in the following sections. The phase diagram of the AT model on a regular d-dimensional lattice in the mean-field limit [23] looks similar to Fig. 2(a); however, the important different feature is the emergence of the extended first-order PT lines between the critical point and the CE point. In the mean-field solution on a regular lattice, these extended lines were absent, thus

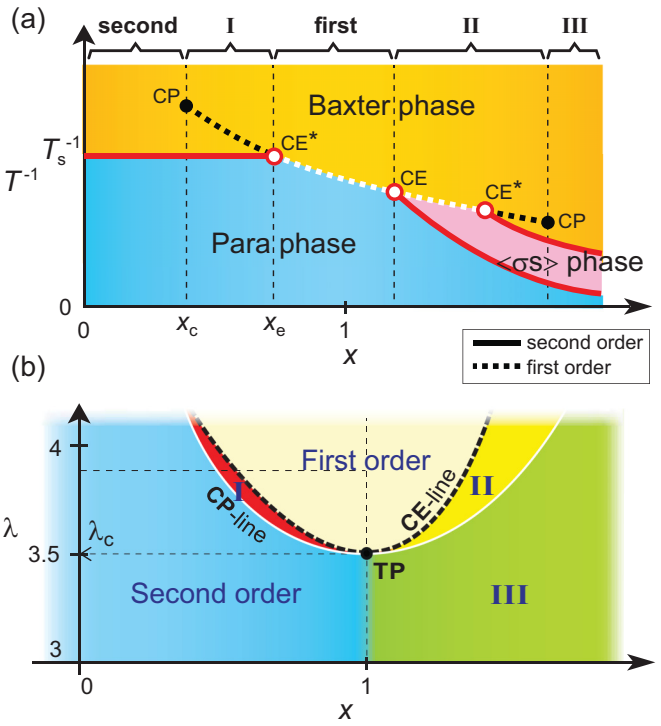

FIG. 2. (Color online) Schematic phase diagram in the spaces (a) (x, T^{-1}) for $\lambda_c < \lambda < 4$ and (b) (x,λ) for $3 < \lambda < 4$. The acronyms are defined as follows: CP, critical point; CE, critical end point; and TP, tricritical point. The upper dashed line in (b) is a guide for the free energy profiles we examine in Fig. 4.

the CE points with asterisks in Fig. 2(a) became tricritical points [23]. On SF networks with $3 < \lambda < 4$, owing to the extended first-order lines, diverse PTs emerge depending on λ and x as shown in Fig. 2(b). For example, different from the tricritical point at which continuous PT occurs, at the CE points the first- and the second-order lines meet, which induces the mixed-order PT; a discontinuous jump in magnetization occurs, but susceptibility diverges as a power law as the second-order PT. In addition, the extended first-order lines induce successive PT, where the continuous PT is followed by a discontinuous PT as temperature decreases. In the following sections we explain the detailed features of the phase diagram and PT patterns for the particular cases $x \equiv K_4/K_2 = 0$ and $x = 1$ first and then for the cases $x < 1$ and $x > 1$.

A. Case $x = 0$ (no interlayer interaction)

When $K_4 = 0$, the AT model reduces to the Ising model on a monolayer network, which shows only continuous PT. This has been extensively studied in various works [24,25]. In this case, the system is ordered for all temperatures for $2 < \lambda \leqslant 3$. The AT model behaves similarly for this range of degree exponent. Thus, we concentrate on the case $\lambda > 3$ in this study. The critical exponents for $3 < \lambda < 5$ are listed in Table I. Here the heat capacity is $C \sim (-t)^{-\alpha}$, for $w \in m, M$ the w magnetization at zero field is $w \sim (-t)^{\beta_w}$, and the susceptibility for w magnetization in the limit $t \to 0^{\pm}$ is $\chi_{w\pm} \sim (\pm t)^{-\gamma_{w\pm}}$, where $t = (T - T_s)/T_s$. In this case, the scaling relation between exponents holds.

TABLE I. Critical exponents for $3 < \lambda < 5$. The heat capacity is $C \sim (-t)^{-\alpha}$, the w magnetization at zero field is $w \sim (-t)^{\beta_w}$, and the susceptibility for w magnetization in the limit $t \to 0^{\pm}$ is $\chi_{w\pm} \sim (\pm t)^{-\gamma_{w\pm}}$, where $t = (T - T_s)/T_s$.

Range of x	α	β_m	β_M	γ_{m-}	γ_{m+}	γ_{M-}	γ_{M+}
$x = 0$	$\frac{\lambda-5}{\lambda-3}$	$\frac{1}{\lambda-3}$		1	1		
$x = 1$ $(\lambda < \lambda_c)$	$\frac{\lambda-5}{\lambda-3}$	$\frac{1}{\lambda-3}$	$\frac{1}{\lambda-3}$	1	1	1	1
$x = 1$ $(\lambda = \lambda_c)$	-1	1	1	1	1	1	1
$0 < x < 1$	$\frac{\lambda-5}{\lambda-3}$	$\frac{1}{\lambda-3}$	$\frac{\lambda-2}{\lambda-3}$	1	1	0	0
$x > 1$ (region III)	$\frac{\lambda-5}{\lambda-3}$	$\frac{1}{\lambda-3}$	$\frac{1}{\lambda-3}$	1	1	1	1

B. Case $x = 1$ (balanced interlayer coupling strength)

When $x = K_4/K_2 = 1$, the single spin and spin product become indistinguishable. Then $m = M$ and the AT model is reduced to the four-state Potts model [26]. Expanding the free-energy density (5) up to third order in m gives

$$f \simeq \frac{3}{2}K_2 m^2\langle k\rangle\left(1 - \frac{K_2\langle k^2\rangle}{\langle k\rangle}\right) + (3C_1 - C_2)(K_2 m)^{\lambda-1} + \frac{N_\lambda k_{\min}^{4-\lambda}}{4-\lambda}(K_2 m)^3 + O_{\text{higher}}, \tag{10}$$

where both $C_1 \equiv C_1(\lambda)$ and $C_2 \equiv C_2(\lambda)$ are positive and O denotes higher orders. Definitions for all coefficients C_i are given in Appendix A.

The PT patterns are determined by the sign of $3C_1 - C_2$. When $3C_1 - C_2 > 0$, which occurs for $\lambda < \lambda_c \approx 3.503$, the second-order PT takes place at $T_s \equiv J_2\langle k^2\rangle/k_B\langle k\rangle$ with the critical exponent $\beta_m = 1/(\lambda - 3)$. Then $\alpha = (\lambda - 5)/(\lambda - 3)$ from $C \sim \partial^2 f/\partial^2 t$. When $3C_1 - C_2 < 0$ for $\lambda > \lambda_c$, the first-order PT occurs at T_f $(> T_s)$. Here T_f is the point at which the free energy discontinuously becomes a global minimum at a finite m. When $3C_1 - C_2 = 0$ at λ_c, the continuous transition occurs at T_s, but the critical exponent differs as $\beta_m = 1$ and $\alpha = -1$. This is the conventional tricritical point (TP), as shown in Fig. 3(h). The susceptibility at the TP also obtained, which diverges at both T_s^+ and T_s^- with the critical exponent $\gamma_m = \gamma_M = 1$.

C. Case $0 < x < 1$ (unbalanced interlayer coupling strength)

When $x = K_4/K_2 \neq 1$, Eqs. (7) and (8) can be expanded in terms of m and M as follows:

$$m\langle k\rangle\left(1 - \frac{T_s}{T}\right) \simeq C_3(K_2 m)^{\lambda-2} + \mathcal{B}_2 + O_{\text{higher}}, \tag{11}$$

$$M\langle k\rangle\left(1 - \frac{xT_s}{T}\right) \simeq C_4(K_4 M)^{\lambda-2} + C_5(K_2 m)^{\lambda-2} + O_{\text{higher}}, \tag{12}$$

where $C_3(\lambda, r_0) < 0$, $C_4(\lambda, r_0) < 0$, and $C_5(\lambda, r_0) > 0$ are numbers of $O(1)$ and they depend on λ and $r_0 \equiv K_4 M/K_2 m$. Here $\mathcal{B}_2(K_2 m, K_4 M, \lambda) > 0$ (defined in Appendix A) and its order depends on the ratio M/m. These expansions are possible near a continuous transition point at which $m > 0$ and $M \ll 1$.

For $x < 1$, as temperature is decreased from a sufficiently large value, the second-order transition for the m magnetization takes place first at T_s because $T_s > xT_s$. Near T_s, the term $1 - xT_s/T$ in Eq. (12) is a number of $O(1)$ and so M and $M^{\lambda-2}$ for $\lambda > 3$ cannot be of the same order. Instead, M and $m^{\lambda-2}$ should be of the same order and they are related as

$$M \simeq \frac{C_5(\lambda, 0)}{\langle k\rangle(1 - xT_s/T)}(K_2 m)^{\lambda-2}. \tag{13}$$

Using Eq. (13), one can show that $\mathcal{B}_2$ is of higher order than $m^{\lambda-2}$. Therefore, from Eq. (11), $m \sim (T_s - T)^{\beta_m}$ with $\beta_m = 1/(\lambda - 3)$ and $M \sim (T_s - T)^{\beta_M}$ with $\beta_M = (\lambda - 2)/(\lambda - 3)$. Then, near this second-order transition point, the heat capacity is given by $C \sim (-t)^{\alpha}$, with $\alpha = (\lambda - 5)/(\lambda - 3)$ from Eq. (14).

The difference in the order of magnitude between m and M, induced by the unbalanced interaction-coupling strength, significantly changes the feature of the free energy compared with that for the $x = 1$ case as follows. Using Eq. (13), we expand the free energy (5) up to the three lowest-order terms with respect to m as

$$f(m) \simeq K_2 m^2\langle k\rangle\left(1 - \frac{T_s}{T}\right) + 2C_1(K_2 m)^{\lambda-1} - \frac{K_4 C_5(\lambda, 0)^2}{2\langle k\rangle(1 - xT_s/T)}(K_2 m)^{2(\lambda-2)} + O_{\text{higher}}. \tag{14}$$

Here the $(\lambda - 1)$-order term is always positive, whereas the $2(\lambda - 2)$-order term is negative. Therefore, the transition nature is not determined only by the sign of the $(\lambda - 1)$-order term as usual. However, competition between the magnitudes of $(\lambda - 1)$- and higher-order terms produces an interesting PT for $\lambda_c < \lambda < 4$. Note that the coefficient of the $2(\lambda - 2)$-order term varies depending on T, x, and λ.

When $\lambda_c < \lambda < 4$, the qualitative feature of the phase diagram is insensitive to λ. Thus, we consider the free energy as a function of x and T. First, we sketch the behavior of $f(m)$ vs m for different values of x. When x is close to zero, the $2(\lambda - 2)$-order term is negligible compared with the $(\lambda - 1)$-order term and the global minimum is located at $m = 0$ for $T \geqslant T_s$ [Fig. 4(a)]. When T is decreased below T_s, the m position of the global minimum increases continuously, which leads to a continuous transition. On the other hand, when x is close to one, the $2(\lambda - 2)$-order term can make a global minimum of $f(m)$ at a certain finite $m \equiv m_2$ for $T \leqslant T_f$, where $T_f > T_s$. Then a discontinuous transition takes place at T_f [Fig. 4(e)].

In the intermediate regime I, which is equal to $[x_c, x_e]$, as temperature is decreased across T_s, the free energy exhibits a global minimum at $m_1(T) > 0$, which increases continuously as the temperature is lowered further. In the meantime, a local minimum of $f(m)$ develops at a certain $m_2(T) > m_1(T)$ due to the $2(\lambda - 2)$-order term. As the temperature is lowered further beyond a certain temperature, denoted by T_f $(< T_s)$, the local minimum at m_2 becomes a global minimum, as depicted in Fig. 4(c). That is, $f(m_2(T_f^-)) < f(m_1(T_f^-)) < 0$. Accordingly, the magnetization jumps discontinuously from m_1 to m_2 at T_f. Thus, the system exhibits a discontinuous transition at T_f. Such successive PTs occur in the intermediate regime of x.

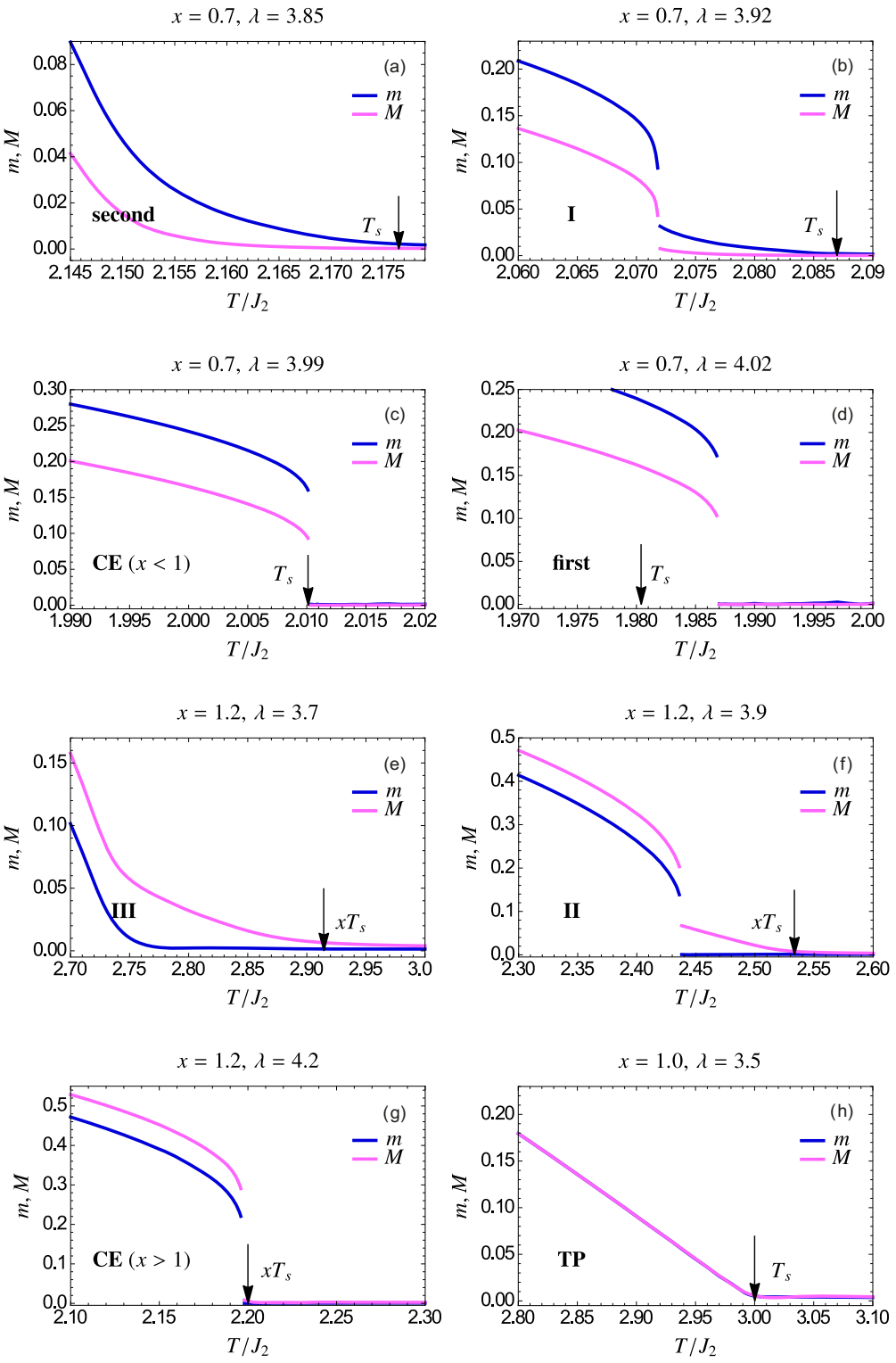

FIG. 3. (Color online) Plot of the order parameter vs temperature $T = K_2^{-1}$ (setting $k_B = 1$) for some particular cases based on numerical values, obtained from Eqs. (5), (7), and (8) by direct integration. The parameter space (x,λ) is specified for each case.

Next we consider particular points at the boundaries of the regime I in Fig. 2(a). The first-order line terminates at a certain point x_c, which is called the critical point, as seen in a liquid-gas system. At this point, the transition is continuous and the behavior of $f(m)$ is shown in Fig. 4(b). On the other hand, the second-order line terminates at a point called the CE point, where the first-order line continues into the regime $x > x_e$. This CE point occurs at temperature T_s, at which there exist two minima in the free-energy function at $m = 0$ and m_2 ($m_2 > 0$), but $f(m) = f(m_2) = 0$ as shown in Fig. 4(d). Thus, $T_f = T_s$. At T_s^+, the magnetization is zero, but at T_s^-, which is equivalent to T_f^-, the

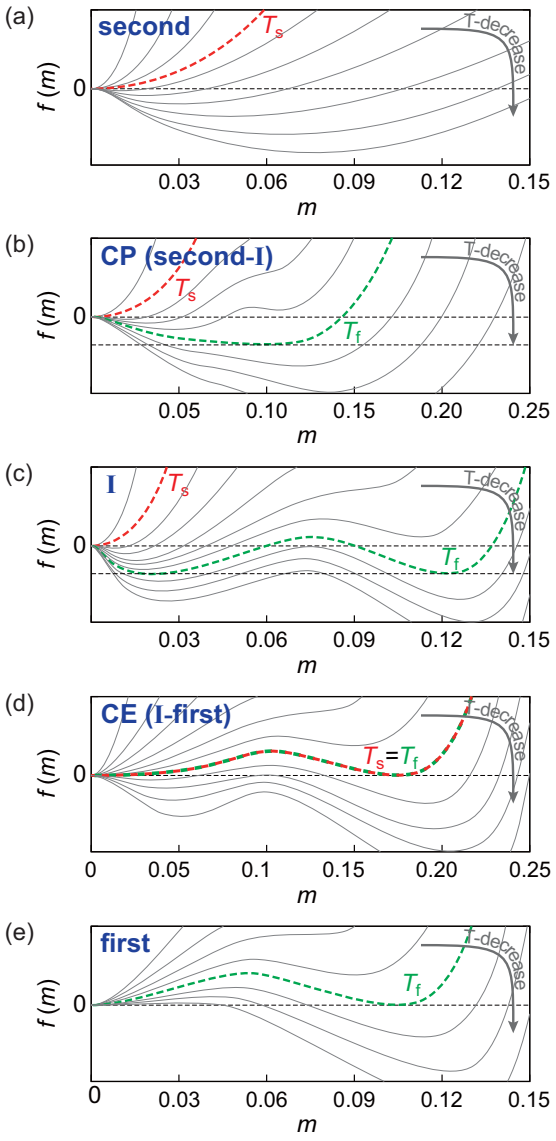

FIG. 4. (Color online) Plots of free energies $f(m)$ vs m for several cases. Suppose that we take a fixed $\lambda = 3.88$ and increase the x value from 0.6 to 0.8 in Fig. 2(b). (a) When $x < x_{\rm CP} \approx 0.71$, the free energy exhibits a global minimum at $m = 0$ for $T \geqslant T_s$ and a finite $m > 0$ for $T < T_s$, which increases gradually as T is decreased beyond T_s. The PT is continuous. (b) At a critical point $x_{\rm CP}$, as temperature is lowered further beyond T_s, a local minimum develops at m_2 besides a global minimum of $f(m)$. At T_f, these two minima merge. The PT is continuous. (c) When x is increased further and is located inside region I, a local minimum at m_2 becomes a global minimum at T_f. Second-order and first-order transitions can take place successively. (d) When $x = x_{\rm CE} \approx 0.77$, there exist two minima in $f(m)$ at $m = 0$ and $m_2 > 0$ and the free energies at these m values are zero. The second derivative of $f(m)$ at $m = 0$ is also zero at T_s. A mixed-order PT takes place. (e) When x is increased further and is located in the first-order region, the second derivative of $f(m)$ at $m = 0$ is not zero and a local minimum at $m_2 > 0$ becomes a global minimum at T_f. A first-order PT takes place.

magnetization jumps to $m_2 > 0$ and the system shows a discontinuous PT.

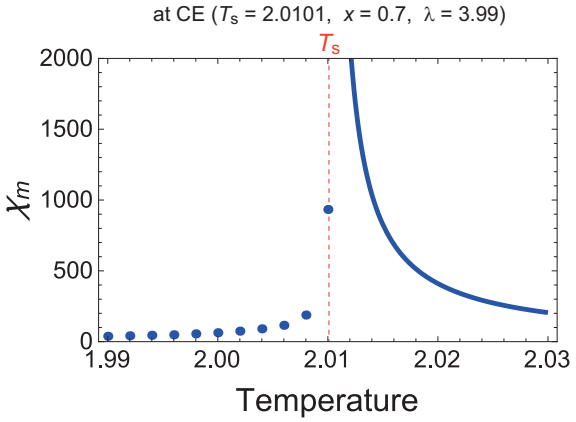

FIG. 5. (Color online) Susceptibility χ_m vs temperature at the CE point. As derived in Eq. (15), χ_m is shown to follow a power law behavior around the temperature T_s, which is indicated with a vertical dashed line.

We also obtain the susceptibility of m magnetization for continuous PT near T_s as

$$\chi_m \approx \begin{cases} \frac{T\langle k^2\rangle}{\langle k\rangle}(T - T_s)^{-1} & \text{for} \quad \mathrm{T} > \mathrm{T_s} \\ \frac{T\langle k^2\rangle}{\langle k\rangle(\lambda-3)}(T_s - T)^{-1} & \text{for} \quad \mathrm{T} < \mathrm{T_s}, \end{cases} \tag{15}$$

which is derived in Appendix B. Thus, the susceptibility exponent is $\gamma_{m\pm} = 1$. Then the scaling relation $\alpha + 2\beta_m + \gamma_{m-} = 2$ holds for m magnetization. This result is valid near any point along the second-order transition line, but not at the CE point. At the CE point, χ_m diverges as Eq. (15) for T_s^+ and becomes finite for T_s^- as shown in Fig. 5 (see Appendix B for detailed calculations). Since the m magnetization is discontinuous but susceptibility χ_m diverges at the CE point, a mixed-order transition emerges at the CE point.

Interestingly, the susceptibility of the M magnetization shows different behavior. Near T_s it is given by

$$\chi_M \approx \frac{T\langle k^2\rangle}{\langle k\rangle(T - xT_s)}. \tag{16}$$

Although the M magnetization exhibits a continuous PT at T_s, the susceptibility does not diverge, that is, $\gamma_{M\pm} = 0$. In addition, the scaling relation for M magnetization does not hold as

$$\alpha + 2\beta_M + \gamma_{M-} = 3 \neq 2. \tag{17}$$

This indicates that the usual scaling hypothesis is not applicable in explaining this scaling phenomenon. This anomaly seems to originate from the scaling effects of H_2 and H_4 fields not being independent of each other. Nevertheless, Eq. (17) satisfies the Rushbrooke inequality $\alpha + 2\beta + \gamma \geqslant 2$ [27].

Consider the phase diagram in the space (x,λ) for $3 < \lambda < 4$ [Fig. 2(b)]. As $\lambda \to \lambda_c^+$, regimes I and II of the successive transitions shrink to the tricritical point at $x = 1$ and λ_c. Remarkably, the upper boundary of regimes I and II becomes a critical end point line on which mixed-order PTs take place.

D. Case $x > 1$ (unbalanced interaction)

When $x > 1$, besides the paraphase and the Baxter phase, the $\langle \sigma s\rangle$ phase also exists. As shown in Fig. 2(a), three

regimes exist: In the first-order transition regime near $x = 1^+$, a discontinuous PT occurs at T_f from the paraphase to the Baxter phase, as depicted in Fig. 3(d). The difference is that M is larger than m. In regime III for $x \gg 1$, M and m undergo the second-order PT at different temperatures xT_s and T_s' $[=T_s/(1-C_6)]$, respectively, as shown in Fig. 3(e). Then the $\langle \sigma s \rangle$ phase exists between xT_s and T_s'. Note that the critical exponent for both magnetizations M and m at xT_s and T_s' is $\beta_M = \beta_m = 1/(\lambda - 3)$. In the intermediate range of x, regime II exists, where more than one type of PT occurs successively as in regime I. In addition, mixed-order PTs also occur at the CE points.

IV. CONCLUSION

In this study we investigated the Ising spin model on a double-layer scale-free network using the AT model in the mean-field approximation. We obtained a rich phase diagram containing diverse types of phase transitions, such as second-order, first-order, successive, and mixed-order PTs, and diverse types of transition points, such as critical, CE, and tricritical points. In particular, CE points exist, as in liquid ^{3}He-^{4}He mixtures [28] and metamagnets [29], at which the mixed-order transitions emerge in the AT model we studied. The rich phase diagram is created as collective phenomena of spins for the asymmetric case ($x \neq 1$) between the intralayer and interlayer interaction strengths. Note that the CE points do not exist but are reduced as a tricritical point for the symmetric case ($x = 1$). We also found the violation of the scaling relation for M magnetization; the proper form of the scaling function should be studied in the future. We anticipate that such a rich phase diagram obtained in thermal equilibrium systems could be a guideline for understanding complex phenomena in multilayer networked systems.

ACKNOWLEDGMENTS

This research was supported by the NRF Grants No. 2011-35B-C00014 (J.S.L.) and No. 2014R1A3A2069005 (B.K.).

S.J. and J.S.L contributed equally to this work.

APPENDIX A: DEFINITIONS FOR COEFFICIENTS

The coefficients C_i and $\mathcal{B}_2$ are defined as follows:

$$C_1(\lambda) = N_\lambda \int_0^\infty \left(-\ln[\cosh y] + \frac{1}{2}y^2 \right) y^{-\lambda},$$

$$C_2(\lambda) = N_\lambda \int_0^\infty \ln[1+\tanh^3 y] y^{-\lambda} dy,$$

$$C_3(\lambda, r_0) = N_\lambda \int_0^\infty \left[\frac{\tanh y}{1+\tanh^2 y \tanh(r_0 y)} - y \right] y^{1-\lambda} dy,$$

$$C_4(\lambda, r_0) = N_\lambda \int_0^\infty \left[\frac{\tanh y}{1+\tanh y \tanh^2(y/r_0)} - y \right] y^{1-\lambda} dy,$$

$$C_5(\lambda, r_0) = N_\lambda \int_0^\infty \frac{\tanh^2 y}{1+\tanh^2 y \tanh(r_0 y)} y^{1-\lambda} dy,$$

$$C_6 = \frac{N_\lambda K_2}{\langle k \rangle} \int_{k_{\min}}^\infty \tanh(K_4 M k) k^{2-\lambda} dk,$$

$$\mathcal{B}_2 = N_\lambda \int_{k_{\min}}^\infty \frac{\tanh(K_2 m k)\tanh(K_4 M k)}{1+\tanh^2(K_2 m k)\tanh(K_4 M k)} k^{1-\lambda} dk. \quad \text{(A1)}$$

APPENDIX B: SUSCEPTIBILITY

With the definitions $\Omega_2 \equiv K_2 m + H_2$ and $\Omega_4 \equiv K_4 m + H_4$, the self-consistent relations for m and M of the AT Hamiltonian with an external field (9) are given as follows:

$$m\langle k \rangle = \int_{k_{\min}}^\infty \frac{\tanh(\Omega_2 k)[1+\tanh(\Omega_4 k)]}{1+\tanh^2(\Omega_2 k)\tanh(\Omega_4 k)} k P_d(k) dk \quad \text{(B1)}$$

and

$$M\langle k \rangle = \int_{k_{\min}}^\infty \frac{\tanh(\Omega_4 k)+\tanh^2(\Omega_2 k)}{1+\tanh^2(\Omega_2 k)\tanh(\Omega_4 k)} k P_d(k) dk. \quad \text{(B2)}$$

First, we consider the susceptibility at the second-order transition point. The self-consistent equation for m (B1) for $x \neq 1$ is expanded with respect to small m and M as

$$m\langle k \rangle \simeq \Omega_2 \langle k^2 \rangle + C_3\left(\lambda, \frac{\Omega_4}{\Omega_2}\right) \Omega_2^{\lambda-2}. \quad \text{(B3)}$$

By taking the partial derivative of the above equation in terms of H_2 and then taking the limit $H_2, H_4 \to 0$, we have

$$\chi_m \langle k \rangle \simeq (K_2 \chi_m + 1)\langle k^2 \rangle + C_3\left(\lambda, \frac{K_4 M}{K_2 m}\right)(\lambda - 2) K_2 \chi_m (K_2 m)^{\lambda-3}, \quad \text{(B4)}$$

where χ_m is the susceptibility of m and is defined as $\frac{\partial m}{\partial H_2}|_{H_2, H_4 \to 0}$. When the second-order phase transition occurs at T_s, $m = 0$ for $T > T_s$ and $C_3(\lambda, \frac{K_4 M}{K_2 m})(K_2 m)^{\lambda-3} \approx \frac{\langle k \rangle}{K_2}(1 - T_s/T)$ for $T < T_s$ near T_s. Then we get (15). Similarly, the self-consistent equation for M (B2) can be expanded as

$$M\langle k \rangle \simeq \Omega_4 \langle k^2 \rangle + C_4\left(\lambda, \frac{\Omega_2}{\Omega_4}\right)\Omega_4^{\lambda-2} + C_5\left(\lambda, \frac{\Omega_4}{\Omega_2}\right)\Omega_2^{\lambda-2}. \quad \text{(B5)}$$

Taking the partial derivative of the above equation by H_4 and then taking the limit $H_2, H_4 \to 0$ gives

$$\chi_M \langle k \rangle \simeq (K_4 \chi_M + 1)\langle k^2 \rangle + C_4\left(\lambda, \frac{K_2 m}{K_4 M}\right)(\lambda - 2) K_4 \chi_M (K_4 M)^{\lambda-3} + C_5\left(\lambda, \frac{K_4 M}{K_2 m}\right) K_2 \frac{\partial m}{\partial H_4}\bigg|_{H_2, H_4 \to 0} (K_2 m)^{\lambda-3}, \quad \text{(B6)}$$

where χ_M is the susceptibility of M and is defined as $\frac{\partial M}{\partial H_4}|_{H_2, H_4 \to 0}$. When the second-order phase transition occurs at T_s, $m = M = 0$ for $T > T_s$ and $(K_2 m)^{\lambda-3} \sim (1 - T_s/T)$ and $M \sim m^{\lambda-2}$ for $T < T_s$ near T_s. Then we get (16).

Second, consider the susceptibility at the critical end point. Since the transition is discontinuous at the critical end point, the expansions with the assumption $m, M \ll 1$ used in the previous derivation is not applicable. Instead, we should keep the explicit integral forms as follows. If we take the derivative of (B1) with respect to H_2 and take the limit $H_2, H_4 \to 0$, we

obtain

$$\chi_m = \frac{\mathcal{A}_1 + \mathcal{A}_2 K_4 (\partial M/\partial H_2)|_{H_2,H_4\to 0}}{\langle k\rangle[1-(K_2/\langle k\rangle)\mathcal{A}_1]}, \tag{B7}$$

where, with $\mathcal{T}_2 \equiv \tanh(K_2 mk)$ and $\mathcal{T}_4 \equiv \tanh(K_4 mk)$,

$$\mathcal{A}_1 = N_\lambda \int_{k_{\min}}^{\infty} \frac{\left(1-\mathcal{T}_2^2\mathcal{T}_4\right)(1+\mathcal{T}_4)}{\left(1+\mathcal{T}_2^2\mathcal{T}_4\right)^2 \cosh^2(K_2 mk)} k^{2-\lambda} dk \tag{B8}$$

and

$$\mathcal{A}_2 = N_\lambda \int_{k_{\min}}^{\infty} \frac{\left(1-\mathcal{T}_2^2\right)\mathcal{T}_2}{\left(1+\mathcal{T}_2^2\mathcal{T}_4\right)^2 \cosh^2(K_4 Mk)} k^{2-\lambda} dk. \tag{B9}$$

To evaluate Eq. (B7) we also should calculate $\partial M/\partial H_2|_{H_2,H_4\to 0}$. If we take the derivative of (B2) with respect to H_2 and take the limit $H_2, H_4 \to 0$, we obtain

$$\left.\frac{\partial M}{\partial H_2}\right|_{H_2,H_4\to 0} = \frac{\mathcal{A}_4(\chi_m K_2 + 1)}{\langle k\rangle[1-(K_4/\langle k\rangle)\mathcal{A}_3]}, \tag{B10}$$

where

$$\mathcal{A}_3 = N_\lambda \int_{k_{\min}}^{\infty} \frac{1-\mathcal{T}_2^4}{\left(1+\mathcal{T}_2^2\mathcal{T}_4\right)^2 \cosh^2(K_4 Mk)} k^{2-\lambda} dk \tag{B11}$$

and

$$\mathcal{A}_4 = N_\lambda \int_{k_{\min}}^{\infty} \frac{2\mathcal{T}_2\left(1-\mathcal{T}_4^2\right)}{\left(1+\mathcal{T}_2^2\mathcal{T}_4\right)^2 \cosh^2(K_2 mk)} k^{2-\lambda} dk. \tag{B12}$$

At the critical end point, $m = M = 0$ for $T > T_s$, so $\mathcal{A}_1 = \langle k^2\rangle$ and $\mathcal{A}_2 = 0$. Then χ_m becomes the same as the result in Eq. (15) for the $T > T_s$ case. For $T < T_s$, χ_m can be numerically evaluated by solving Eqs. (B7) and (B10) together. Through numerical evaluation, we found that the susceptibility becomes finite for $T < T_s$.

[1] S. V. Buldyrev, R. Parshani, G. Paul, H. E. Stanley, and S. Havlin, Nature (London) **464**, 1025 (2010).
[2] M. E. J. Newman, Phys. Rev. E **66**, 016128 (2002).
[3] R. Pastor-Satorras and A. Vespignani, Phys. Rev. Lett. **86**, 3200 (2001).
[4] K. Sznajd-Weron and J. Sznajd, Int. J. Mod. Phys. C **11**, 1157 (2000).
[5] T. M. Liggett, *Stochastic Interaction Systems: Contact, Voter and Exclusion Processes* (Springer, Berlin, 1999), p. 139.
[6] G. J. Baxter, S. N. Dorogovtsev, A. V. Goltsev, and J. F. F. Mendes, Phys. Rev. Lett. **109**, 248701 (2012).
[7] M. Kivela, A. Arenas, M. Barthelemy, J. P. Gleeson, Y. Moreno, and M. A. Porter, J. Complex Networks **2**, 203 (2014), and references therein.
[8] S. Boccaletti, G. Bianconi, R. Criado, C. I. del Genio, J. Gmez-Gardees, M. Romance, I. Sendia-Nadal, Z. Wang, and M. Zanin, Phys. Rep. **544**, 1 (2014).
[9] K.-M. Lee, B. Min, and K.-I. Goh, Eur. Phys. J. B **88**, 48 (2015).
[10] A. Bar and D. Mukamel, Phys. Rev. Lett. **112**, 015701 (2014).
[11] S. N. Dorogovtsev, A. V. Goltsev, and J. F. F. Mendes, Phys. Rev. Lett. **96**, 040601 (2006).
[12] P. M. Kogut and P. L. Leath, J. Phys. C **14**, 3187 (1981).
[13] J. Adler, Physica A **171**, 453 (1991).
[14] M. Aizenman, J. T. Chayes, L. Chayes, and C. M. Newman, J. Stat. Phys. **50**, 1 (1988).
[15] B. C. Coutinho, A. V. Goltsev, S. N. Dorogovtsev, and J. F. F. Mendes, Phys. Rev. E **87**, 032106 (2013).
[16] W. A. Brock and S. N. Durlauf, in *Handbook of Econometrics*, edited by J. J. Heckman and E. E. Leamer (Elsevier, Amsterdam, 2001), Vol. 5, Chap. 54, p. 3297.
[17] N. Masuda, Phys. Rev. E **90**, 012802 (2014).
[18] M. Diakonova, M. San Miguel, and V. M. Eguíluz, Phys. Rev. E **89**, 062818 (2014).
[19] K. Suchecki and J. A. Hołyst, Phys. Rev. E **74**, 011122 (2006).
[20] J. Ashkin and E. Teller, Phys. Rev. **64**, 178 (1943).
[21] S. Bradde, F. Caccioli, L. Dall'Asta, and G. Bianconi, Phys. Rev. Lett. **104**, 218701 (2010).
[22] G. Bianconi, Phys. Rev. E **85**, 061113 (2012).
[23] R. V. Ditzian, J. R. Banavar, G. S. Grest, and L. P. Kadanoff, Phys. Rev. B **22**, 2542 (1980).
[24] G. Bianconi, Phys. Lett. A **303**, 166 (2002).
[25] S. N. Dorogovtsev, A. V. Goltsev, and J. F. F. Mendes, Phys. Rev. E **66**, 016104 (2002).
[26] F. Iglói and L. Turban, Phys. Rev. E **66**, 036140 (2002).
[27] H. E. Stanley, *Introduction to Phase Transitions and Critical Phenomena* (Oxford University Press, Oxford, 1987).
[28] E. H. Graf, D. M. Lee, and J. D. Reppy, Phys. Rev. Lett. **19**, 417 (1967).
[29] J. M. Kincaid and E. G. D. Cohen, Phys. Rep. **22**, 57 (1975).